Determination of Center of Rotation in Computed Tomography

David Hägele

Abstract—This paper will discuss the aspect of the determination of center of rotation in computed tomography. An introduction to computed tomography imaging will be given in the beginning as a prerequisite to the actual topic. This will cover different geometries (parallel beam, fan beam and cone beam), which are present in computed tomography and used to model the projection space of a CT-scan, as well as basic knowledge about tomographic reconstruction, including the Fourier slice theorem and filtered back projection. The problem of wrong center of rotation assumption in tomographic reconstruction will be explained, which has the effect of image degradation. Different solutions to the determination of the correct location of the center of rotation found in the literature will be presented. It is found that the approaches can be split into sinogram and reconstruction based methods, where sinogram based methods analyze the sinogram that is the product of a CT-scan, while reconstruction based methods analyze reconstructed images of different centers of rotation to find the correct one. Finally a conclusion summarizing the paper will be drawn.

Index Terms—Computer Science, Image Processing, Computed Tomography, Tomographic Reconstruction

1 Introduction

In computed tomography (CT), a set of set of projections is acquired by meassuring the attenuation of X-rays through the scanned object at different rotation angles. The X-rays are emmited by a source on one side of the scanned object, intersect with the object, and hit a detector on the other side. The resulting measurement of the detector is a projection of the object's internals. Rotating the object and repeating the process results in a set of projections, which can be used to reconstruct an image of the internal structure of the scanned object. For this reconstruction it is mandatory to know the center of rotation (COR), or rather the location of its projection, as slight deviations from the actual COR produce severe artifacts in the reconstructed image. In general, the COR is assumed to be projected onto the center of the detector, but this assumption can be violated on badly calibrated CT systems. A correct calibration can also become almost impossible when the X-ray source is very close to the scanned object, as is the case for industrial scanners with resolutions on the micrometer scale [1]. In this paper, different techniques and algorithms for the determination of the center of rotation are explained, which can be found in the literature.

2 Prerequisites

In order to explain the problem of inaccurate COR assumption in tomographic reconstruction, some prerequisite knowledge about CT will be briefly explained in this section.

2.1 Image Acquisition in CT

This subsection will briefly explain how images are typically acquired in CT.

In X-ray imaging, an X-ray source (e.g. X-ray tube) is used to generate photons which then run through an object. The capability of the photons to penetrate matter, depends on the material, which means that the decrease in number of photons along the incident beam is different for different materials. The decrease in the number of photons, or attenuation, results from the photons being absorbed or scattered as they travel through the matter [2]. Using an X-ray detector, the photon count after matter penetration can be measured and thus the attenuation along the beam from the source to the detector. The measured quantity can be interpreted as the projection of all attenuations along the ray.

However, a single projection is not sufficient to deduce the attenuation strengths within the object. To locate regions of high and low attenuation, multiple projections from different sides of the object are required. Therefore the object is placed on a rotary table or the imaging aparatus (X-ray source and detector) is rotated around the object.

2.2 CT Geometries

This subsection will briefly explain the most common geometries in CT, that is the setup of X-ray source and detector and the ray projections which result from it.

2.2.1 Parallel Beam

The simplest geometry in CT (from a mathematical point of view) is the parallel beam geometry. Here all rays are parallel that are emitted from the same side of the object. Figure 1a shows a schematic of this geometry with the resulting signal.

This projection geometry can be mathematically expressed with the Radon transform. When we think of the object as a function of attenuation coefficients $f(x, y)$ and the measured signal as a function of projected coefficients $R(r, \gamma)$ where r is the position on the detector and γ is the rotation angle at which the signal is obtained, then

$$R(r,\gamma) = \int_{-\infty}^{\infty} f(r\ cos(\gamma) + t\ sin(\gamma), r\ sin(\gamma) - t\ cos(\gamma))\ dt. \tag{1}$$

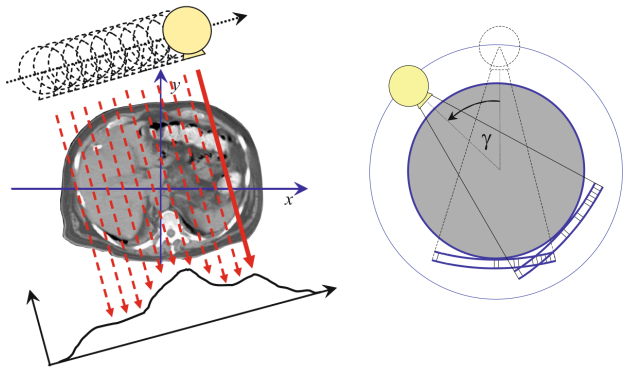

(a) Parallel Beam (b) Fan Beam

Fig. 1. Parallel beam and fan beam geometry. In parallel beam the source moving perpendicular to the ray direction for sampling a 1-dimensional image (graph). In fan beam, rays are not perpendicular but instead emitted in fan blade form. γ is the rotation angle at which the signal is obtained. Figures from [3], [4]

The parameter t is the position on the ray that hits the detector at r and angle γ, which makes it clear that the projection $R(r, \gamma)$ is the integral along a ray through the object $f(x, y)$. The sampling of an object in this fashion, results in a so called sinogram. The contribution of a specific area of the object to the individual projections, follows a sinusoidal path along the γ-axis as can be seen in fig. 2

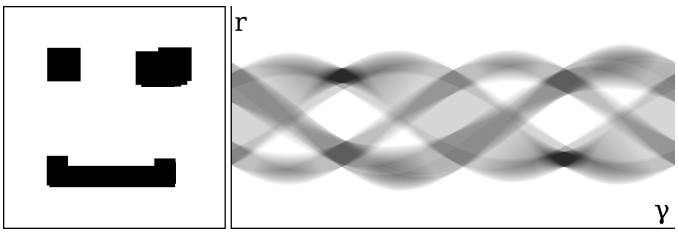

Fig. 2. A "smilie" phantom and its corresponding sinogram with $\gamma \in [0°, 360°]$. An imaginary CT would have started with source on top and detector on bottom and then rotated clockwise around the phantom to obtain the shown sinogram.

Unfortuantely, parallel beam geometry is impractical as a pencil beam X-ray source (source emitting only one ray in a specific direction) would have to be moved parallel to the detector to collect all samples for a single rotation angle, which is very time consuming [5]. However, parallel beam geometry occurs at synchrotron facilities [**?**].

2.2.2 Fan Beam

A more practical geometry is the fan beam, in which a source emits a flat beam that extends to the sides (like a fan blade). Figure 1b shows a schematic of this geometry. Here the projection for a single rotation angle can be obtained at once. The geometry can be defined by the COR it rotates around, the offset of the source to the COR and its aperture angle. In clinical practice curved detector rays are used, as shown in fig. 1b, to get constant aperture angle steps for each detector cell.

As each ray projection for a single rotation angle in this geometry corresponds to a different ray directions (i.e. rays are not parallel here), the resulting sinogram differs from

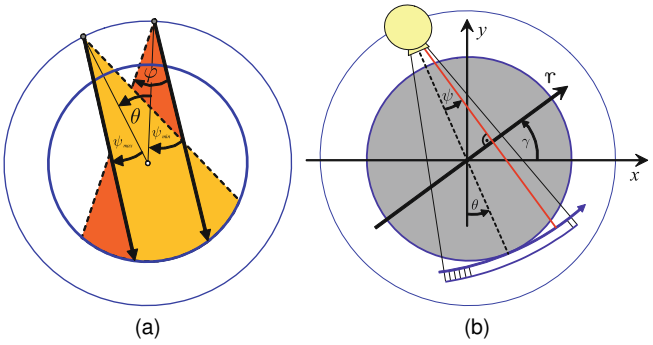

(a) (b)

Fig. 3. On the left a schematic is shown with two fan beams with aperture angle φ at different rotation angles. It can be sen that the outer rays of the two are parallel. The maximum distance of two parallel beams is limited by φ, and the maximum rotation angle θ at which two parallel rays can be obtained is given by $\theta = \psi_{min} + \psi_{max}$ which are the angles from central to outer rays. On the right a schematic is shown that points out the correspondence between fan and parallel beam geometry. It can be seen that for the red ray which is the ray at rotation angle θ with deviation angle ψ from the central ray, there exists an angle γ in parallel beam geometry so that it is perpendicular to the r-axis (i.e. parallel beam detector). Figures from [5]

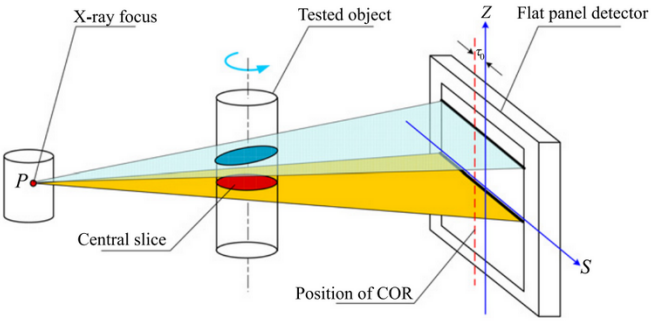

Fig. 4. A cone beam setup with an object on a rotary table. It can be seen that only the projection of the central slice is equivalent to a projection in fan beam geometry. Other projections that are parallel to the s-axis of the detector use samples at multiple heights of the object. Also the projection of the rotation axis onto the detector is shown which in this case is offset from detectors z-axis. Figure from [6]

the sinogram of parallel beam geometry. When analyzing this geometry further, it can be seen that the ray projections of a parallel beam geometry are inherent and can be found at different rotation angles. Through a process called rebinning, the sinogram of the fan beam can be transformed to parallel beam. Figure 3 illustrates this concept.

2.2.3 Cone Beam

The previously introduced geometries are both 2-dimensional (2D) as they described projections within an x-y-plane onto a one dimensional detector. To obtain a 3-dimensional (3D) image the scanned object would have to be moved perpendicular to the plane to obtain multiple slice images. With the 3D cone beam geometry, this is not necessary as it uses a cone shaped beam that projects onto a 2D flat panel detector. In fig. 4 it can be seen that there exists a certain line on the detector which will receive the same input as a fan beam detector. All other lines read projections through multiple planes of the object and are thus not rebinnable to parallel beam.

2.3 Reconstruction

This subsection will explain the process of reconstructing an image from the projections obtained in CT. Only the 2D case will be explained as it is relevant for understanding the COR determination techniques later on. Also this subsection will only cover Fourier based reconstruction, especially filtered back projection.

The problem of reconstruction can be stated as follows. Given the Radon transform from eq. (1) $R(r,\gamma)$ how do we calculate the original signal $f(x,y)$? The solution to this would be the inverse Radon transform $R(r,\gamma)^{-1}$. To solve this, the Fourier slice theorem can be leveraged.

$$p(x) = R(x,0) = \int_{-\infty}^{\infty} f(x,y)\ dy. \tag{2}$$

$$\hat{f}(u,v) = \int_{-\infty}^{\infty}\int_{-\infty}^{\infty} f(x,y)e^{-2\pi i(xu+yv)}\ dx\ dy. \tag{3}$$

$$\begin{aligned} s(u) = \hat{f}(u,0) &= \int_{-\infty}^{\infty}\int_{-\infty}^{\infty} f(x,y)e^{-2\pi ixu}\ dx\ dy \\ &= \int_{-\infty}^{\infty}\left[\int_{-\infty}^{\infty} f(x,y)\ dy\right] e^{-2\pi ixu}\ dx \\ &= \int_{-\infty}^{\infty} p(x)e^{-2\pi ixu}\ dx = \hat{p}(u). \end{aligned} \tag{4}$$

The proof of the Fourier slice thoerem above (eq. (4)) states that the Fourier transform $\hat{p}(u)$ of a projection $p(x)$ of $f(x,y)$, is the same as the slice $s(u)$ (parallel to the projection line and through the center) of the Fourrier transform $\hat{f}(u,v)$ of $f(x,y)$. In short $s(u) = \hat{p}(u)$.

As th Radon transform is a set of projections the Fourier slice theorem can be used to build the Fourier tranform of the original signal and reconstruct it using the inverse Fourier transform. Figure 5 illustrates this method. The problem of applying this algorithm in practice is, that due to the limited angular resolution (i.e. discretization) of the Radon transform the frequency information density in the Fourier space decreases for higher frequencies [7]. In the process of cartesian regridding of the polar coordinates a lot of data for the high frequencies would have to be made up in order to perform an inverse fast Fourier transform. Therefore a different algorithm, the filtered back projection, is used in practice.

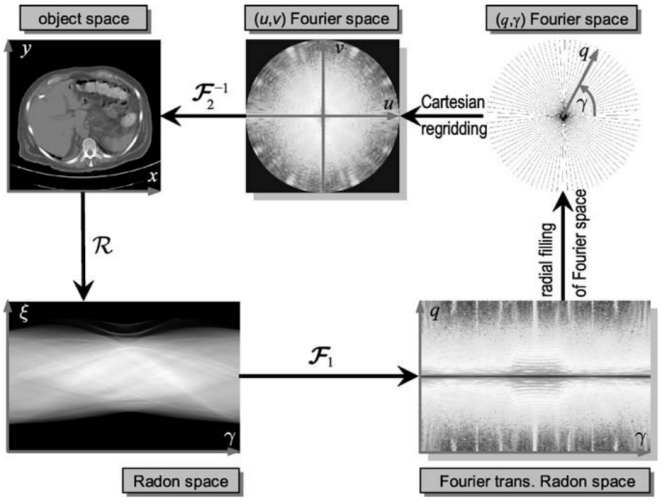

Fig. 5. The inverse Radon transform can be calculated using the Fourier slice theorem. First all projections are transformed to the Fourier space along the ξ-axis ($= r$-axis). Then the Fourier transform is built by placing all transformed projections according to their angle into a polar coordinate system. The coordinate system thus consists of slices of the Fourier transform of the original signal which can then be obtained using an inverse Fourier transform. Figure from [7]

2.3.1 Filtered Back Projection

The back projection algorithm reconstructs the original image from a discrete radon transform (i.e. parallel beam sinogram). For the reconstruction of a single pixel, the information has to be gathered from the ray projections of the rays that intersect this pixel (see eq. (5)).

$$g(x,y) = \int_0^{\pi} R(x\ cos(\gamma) + y\ sin(\gamma), \gamma)\ d\gamma. \tag{5}$$

This can be imagined as smearing the projections over a canvas in their respective directions. At first glance this may seem as the correct inversion of the projections but is not. This becomes clear when thinking about the original image being a Dirac delta (image with all entries zero except for the central pixel). The projections of this image will be 1D Dirac deltas, but using the back projection algorithm will not restore the 2D Dirac but instead smear the 1D Diracs also into areas which are supposed to be zero. In fact the resulting image looks quite blurry which is due to the back projection equaling to the original image convolved with the point spread function of the imaging system (i.e. the Radon transform) $\frac{1}{|(x,y)|}$ [7]. To counter this, the projections first need to be filtered with a high pass filter. This introduces negative values in the projections which in the back projection process cancel out positive contributions of other projections. Figure fig. 6 shows the results of unfiltered and filtered back projection. As amplifying high frequencies also amplifies noise, there are different filters that can be used in practice [8].

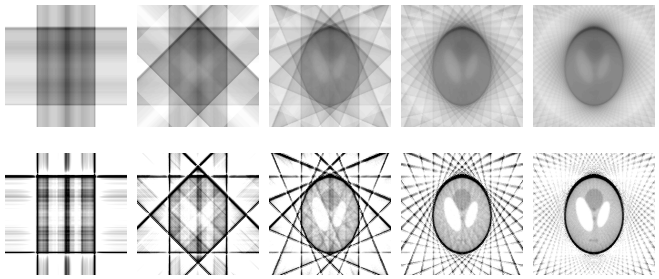

Fig. 6. On the top row, the results of unfiltered back projection are shown. From left to right the number of projections used increases from 2 to 32. The resulting image looks blurry. On the bottom row the results of filtered back projection are shown. The resulting image looks quite crips and edges are clearly visible. The Shepp Logan phantom [9] was used as source image.

3 COR Determination

The problem of incorrect assumption of the location of the COR can occur in CT setups with misaligned source and detector. Especially in industrial CT with resolutions on the micrometer scale, calibrating a CT system correctly can be

very challenging. In parallel beam geometry, a misaligned COR, i.e. the COR is projected onto τ on the r-axis, results in a shift of the sinogram along the r-axis by τ.

$$R_\tau(r, \gamma) = R(r - \tau, \gamma) \tag{6}$$

The actual problem arises when reconstructing the signal from R_τ as the algorithms, e.g. filtered back projection (FBP), assume the COR to be in the center. Thus, ray intersections do not lign up correctly and the reconstructed image suffers from streaking artifacts. Figure 7 shows the effect of shift of COR in FBP.

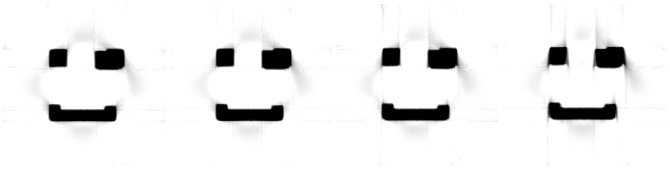

(a) $\tau = 0$px (b) $\tau = 2$px (c) $\tau = 4$px (d) $\tau = 8$px

Fig. 7. FBP of the phantom from fig. 2 with different shifts (τ) of COR. The resolution of the sinogram in r direction was 256 pixels. With incresing shift, stronger vertical streaking artifacts are introduced into the reconstructed image.

In order to correctly reconstruct the signal, the COR first need to be determined. Several approaches to this problem can be found in the literature, which will be introduced in the following subsections. The variety of approaches can subdivided in sinogram base methods, which analyze a sinogram in order to find the COR, and reconstruction based methods, which compare reconstruction results with different COR in an iterative fashion.

3.1 Sinogram Based Methods

In this subsection the approaches that are based on sinogram analysis are introduced. The approaches are presented in chronological order.

3.1.1 High Density Feature

Crawford et al. [10] presented an approach for finding the COR in which they used two $180°$ opposing projections of a distinct high density feature. When locating this feature in the two projections, the COR can be calculated as the sum of the detector coordinates of the feature divided by two. This becomes clear when thinking about the feature being offset from the COR by δ in projection p_1. The corresponding position of the feature in projection p_2 will then be on the opposite side of the COR, offset by $-\delta$ from the COR. Figure 8 illustrates this concept.

This approach could also be expanded to use all projections in the sinogram. For each opposing pair of projections the COR could be calculated and then the mean of all CORs will yield the final result. This approach can be automated if there exists a distinct global maximum in the projections of the sinogram, otherwise a location of the correct feature is not guaranteed.

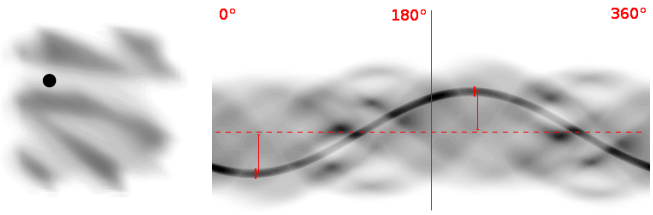

(a) phantom (b) sinogram

Fig. 8. A phantom with a high density feature is shown on the left side. In corresponding sinogram on the right, the sinusodial trace of the feature can be observed. The dotted line indicates the COR in the sinogram. It can be seen that the feature locations in $180°$ opposing projections have the same distance to the COR.

3.1.2 Center of Mass

Azevedo et al. [1] proposed a more generally applicable algorithm, in which they replaced the high density feature from [10] with the center of mass. The center of mass of the original signal is a point $(\overline{x}, \overline{y})$ which's coordinates can be calculated as follows (calculation of $\overline{y}$ analogous to $\overline{x}$).

$$\overline{x} = \frac{\int_{-\infty}^{\infty}\int_{-\infty}^{\infty} x\ f(x,y)\ dx\ dy}{\int_{-\infty}^{\infty}\int_{-\infty}^{\infty} f(x,y)\ dx\ dy} \tag{7}$$

As the center of mass of the original signal $f(x, y)$ is projected onto the projection center of mass in parallel beam geometry, it can be used as a reference feature. The projection center of mass is dependent on the projection angle and can be calculated as follows.

$$\overline{r_\tau}(\gamma) = \frac{\int_{-\infty}^{\infty} r\ R_\tau(r,\gamma)\ dr}{\int_{-\infty}^{\infty} R_\tau(r,\gamma)\ dr} = \frac{\int_{-\infty}^{\infty} r\ R(r-\tau,\gamma)\ dr}{\int_{-\infty}^{\infty} R_(r-\tau,\gamma)\ dr} \tag{8}$$

where $R_\tau(r, \gamma)$ is the radon transform with COR offset by τ (eq. (6)). The previous equation can be simplified to the following.

$$\overline{r_\tau}(\gamma) = \tau + \overline{r}(\gamma) = \tau + \overline{x}\ cos(\gamma) + \overline{y}\ sin(\gamma) \tag{9}$$

Using linear regression (least squares) the parameters τ, $\overline{x}$ and $\overline{y}$ can be approximated from the matrix notation of eq. (9).

$$\begin{pmatrix} 1 & cos(\gamma_1) & sin(\gamma_1) \\ \vdots & \vdots & \vdots \\ 1 & cos(\gamma_n) & sin(\gamma_n) \end{pmatrix} \cdot \begin{pmatrix} \tau \\ \overline{x} \\ \overline{y} \end{pmatrix} = \begin{pmatrix} \overline{r_\tau}(\gamma_1) \\ \vdots \\ \overline{r_\tau}(\gamma_n) \end{pmatrix} \tag{10}$$

Even though $\overline{x}$ and $\overline{y}$ are not needed for a correct reconstruction, it is a neat bonus.

Azevedo et al. showed that their algorithm is quite robust against Gaussian noise and isolated singularities [1]. Unfortunately their algorithm is not applicable to fan beam geometry in general the objects center of mass is no longer projected onto the projections center of mass as was the case for parallel beam. However for an object function $f(x, y) = \delta(x - \overline{x}, y - \overline{y})$, that is a Dirac delta function translated by $(\overline{x}, \overline{y})$, the center of mass is projected onto the projections center of mass. Therefore this method can be used for calibration (i.e. finding the COR beforehand) using an object that approximates a Dirac delta like a thin wire or pin phantom.

3.1.3 Cross-Correlation

Yang et al. [6] proposed another sinogram based method for COR determination using image cross-correlation. Given a sinogram in a parallel beam geometry over $360°$ (which can also be obtained by rebinning a fan-beam sinogram), the sinogram is divided in half so that both halfs cover a $180°$ range. As the information in both sub sinograms is redundant in that way that they are mirror images of each other, flipping one of them will result in two sinograms over $180°$ with identical information.

$$R(r,\gamma)^{[0,\pi]} = R(-r,\gamma)^{[\pi,2\pi]} \tag{11}$$

A shift of COR, as explained in the beginning of section 3, results in a shift of the sinogram along the r-axis (see eq. (6)). Thus, the two sub sinograms are identical under this shift.

$$R_\tau(r+\tau,\gamma)^{[0,\pi]} = R_\tau(-(r+\tau),\gamma)^{[\pi,2\pi]} \tag{12}$$

Using the 1D cross correlation of the two sinograms along the r-axis, the shift can be determined as follows.

$$2\tau = \underset{r}{arg\,max} \quad R_\tau(r,\gamma)^{[0,\pi]} \star R_\tau(-r,\gamma)^{[\pi,2\pi]} \tag{13}$$

The authors [6] provided evidence that their algorithm is robust against Gaussian noise even for large variance values. They also stated that their algorithm can be used for 3D CT with cone beam geometry when using the central slice (see section 2.2.3). As locating the central slice is not trivial and depends on calibration as well, it was shown that the algorithm still performs well for sinograms that slightly deviate from that of the central slice.

3.2 Reconstruction Based Methods

Reconstruction based methods, as opposed to sinogram based methods, use an iterative approach to finding the COR. The individual steps of an iterative algorithm are:

1) reconstruct image with COR τ_i
2) generate a score for the reconstructed image that indicates the quality of the reconstruction, and thus the correctness of τ_i
3) repeat for different τ_i
4) select τ_i with best score as correct COR

This process is of course very time consuming due to the repeating reconstruction step, but is not dependent on specific CT geometries. The crucial part of this algorithm is the generation of a score, which requires an image metric $Q(\tilde{f})$ to assess the quality of the reconstructed image $\tilde{f}$. In the following two different metrics are introduced.

3.2.1 Integral of Negativity

As proposed by Donath et al. [11] the integral of negativity can be leveraged to build an image metric Q_{IN}.

$$Q_{IN}(\tilde{f}) = -\frac{1}{m_0} \int_{-\infty}^{\infty}\int_{-\infty}^{\infty} \varepsilon(-\tilde{f}(x,y))\,\tilde{f}(x,y)\,dx\,dy. \tag{14}$$

$$m_0 = \int_{-\infty}^{\infty}\int_{-\infty}^{\infty} f(x,y)\,dx\,dy = \int_{-\infty}^{\infty} R(r,\gamma_0)\,dr \tag{15}$$

$$\varepsilon(a) = \begin{cases} 1: & a \geq 0 \\ 0: & else \end{cases} \quad \text{(Heaviside function)} \tag{16}$$

Q_{IN} is calculated as the ratio of the integral of negativity of the reconstructed image to the zeroth order moment m_0 (total mass) of the original signal. Fortunately the original image does not need to be known in order to calculate m_0, it is the integral of along the r-axis of any projection of the sinogram.

Recalling the filtering step in FBP where negative projection values are introduced to cancel out positive contribution (see section 2.3.1), it makes sense to analyze the negativity of the reconstructed image. In a perfect reconstruction the negativity would be zero as the original image had no negative values, so minimizing this metric yields the correct COR.

Brunetti and De Carlo [12] used a similar metric in their work based on the number of negative values in the reconstructed image.

3.2.2 Histogram Entropy

As pointed out by Donath et al. [11], the metric Q_{IN} can only be used for non-negative object functions. Therefore they provided another metric based on the histogram entropy that is also applicable when negative attenuation coefficients are present (which can occur when samples are recorded in a surrounding medium e.g. water [11]). They defined a metric Q_H as follows.

$$Q_H(\tilde{f}) = \frac{H}{H_{max}} \tag{17}$$

$$H = -\int_{-\infty}^{\infty} p(g)\,log_2(h\,p(g))\,dg \tag{18}$$

Here the metric is build by normalizing the entropy H by the maximum entropy H_{max}. H is a continuous version of the discrete entropy for gray-level images, where $p(g)$ is an estimate probability density function for continuous gray levels g and h describes the density resolution.

The reasoning for the correctness of this metric is based on the assumption that the reconstructed image consists of homogenious regions, which is at least true for the outer regions that are zero. In a reconstruction with wrong COR, additional structures are introduced which smear out the histogram.

4 Conclusion

In this paper about the determination of the COR in CT, a brief introduction was given about image acquisition in CT in the beginning (section 2.1). Several CT geometries were introduced; the parallel beam geometry (section 2.2.1) which is mathematically described by the Radon transform and which most of the COR determination algorithms assume; the fan beam geometry (section 2.2.2) which is more common and can be transformed to a parallel beam geometry; and the cone beam geometry (section 2.2.3) which, in contrast to the former, is a 3D geometry. In the last part of the introduction to CT imaging, the reconstruction was discussed (section 2.3) in which the Fourier slice theorem was explained as well as the filtered back projection (section 2.3.1) as a representative reconstruction algorithm.

In the following section the key topic of this paper was addressed. Firstly the problem of inaccurate or wrong COR assumption for reconstruction was explained (section 3)

which is the image degradation due to artifacts. Afterwards the different methods for COR determination found in the literature were presented which can be classified into sinogram based methods and reconstruction based methods.

The sinogram based methods comprise the high density feature tracing method (section 3.1.1), in which a pin phantom can be used to create a distinct sinusodial trace in the sinogram from which the actual COR can be deduced; the center of mass method (section 3.1.2) which is also applicable without the use of a special phantom as it uses the objects center of mass as a tracing point; and the cross-correlation method (section 3.1.3) which leverages the redundant information in the upper and lower half of a sinogram over $360°$.

In the section of reconstruction based methods a basic iterative algorithm was introduced (section 3.2) which uses uses an image metric to judge the quality of a reconstructed image. Following that, two image metrics were presented that could be used in the algorithm, which are the integral of negativity metric (section 3.2.1) and the histogram entropy metric (section 3.2.2).

REFERENCES

[1] S. G. Azevedo, D. J. Schneberk, J. P. Fitch, and H. E. Martz, "Calculation of the rotational centers in computed tomography sinograms," *IEEE Transactions on Nuclear Science*, vol. 37, no. 4, pp. 1525–1540, Aug 1990.

[2] T. Buzug, *Computed Tomography*. Berlin, Heidelberg: Springer Berlin Heidelberg, 2008, ch. Fundamentals of X-ray Physics, pp. 15–73.

[3] ——, *Computed Tomography*. Berlin, Heidelberg: Springer Berlin Heidelberg, 2008, ch. Milestones of Computed Tomography, pp. 75–99.

[4] ——, *Computed Tomography*. Berlin, Heidelberg: Springer Berlin Heidelberg, 2008, ch. Fundamentals of Signal Processing, pp. 101–150.

[5] ——, *Computed Tomography*. Berlin, Heidelberg: Springer Berlin Heidelberg, 2008, ch. Technical Implementation, pp. 241–301.

[6] M. Yang, H. Gao, X. Li, F. Meng, and D. Wei, "A new method to determine the center of rotation shift in 2d-ct scanning system using image cross correlation," *NDT & E International*, vol. 46, pp. 48 – 54, 2012.

[7] T. Buzug, *Computed Tomography*. Berlin, Heidelberg: Springer Berlin Heidelberg, 2008, ch. Two-Dimensional Fourier-Based Reconstruction Methods, pp. 151–200.

[8] T. H. Farquhar, A. Chatziioannou, G. Chinn, M. Dahlbom, and E. J. Hoffman, "An investigation of filter choice for filtered backprojection reconstruction in pet," *IEEE Transactions on Nuclear Science*, vol. 45, no. 3, pp. 1133–1137, 1998.

[9] L. A. Shepp and B. F. Logan, "The fourier reconstruction of a head section," *IEEE Transactions on Nuclear Science*, vol. 21, no. 3, pp. 21–43, 1974.

[10] C. R. Crawford, G. T. Gullberg, and B. M. W. Tsui, "Reconstruction for fan beam with an angular-dependent displaced center-of-rotation," *Medical Physics*, vol. 15, no. 1.

[11] T. Donath, F. Beckmann, and A. Schreyer, "Automated determination of the center of rotation in tomography data," vol. 23, 06 2006, pp. 1048–57.

[12] A. Brunetti and F. De Carlo, "A robust procedure for determination of center of rotation in tomography," vol. 5535, 2004, pp. 652–659.